arXiv:0812.0757v1 [hep-ex] 3 Dec 2008

Jet substructure at HERA*

Claudia Glasman[a] (*On behalf of the H1 and ZEUS Collaborations*)

[a]Universidad Autónoma de Madrid,
Departamento de Física Teórica, Facultad de Ciencias
Cantoblanco, E-28049 Madrid, Spain

A review is presented of jet substructure measurements from the H1 and ZEUS Collaborations at HERA. The results presented include tests of perturbative QCD, comparison of the properties of quark and gluon jets, the comparison of the pattern of QCD radiation in different hard scattering processes, determination of the strong coupling and studies of the underlying subprocesses dynamics and of the pattern of parton radiation.

1. Introduction

Perturbative calculations deal only with partons in the final state. However, hadrons and not partons are observed in the detector. The hadrons are the result of the fragmentation of the partons such that all the hadrons originating from a given parton are contained in a narrow region around the direction of the original parton, what is commonly called a jet. Therefore, the first step in comparing data and theory is to reconstruct the parton topology. This is best done with jet algorithms, which define the jets in a very specific way. The jets obtained display the following characteristics: *(i)* the longitudinal momentum (p_L) distribution of the hadrons in a jet should scale with the jet energy; *(ii)* the transverse momentum (p_T) distribution of the hadrons should have a mean value of about 300 MeV. Thus, the mean angle ($\sim p_T/p_L$) between a hadron and the jet axis and the size of a cone which contains a constant fraction of energy will decrease with increasing jet energy. At high energies, this picture is modified since gluon emission from the original parton overcomes the fragmentation effects and so the structure of the jets is driven by radiation, which has the advantage of being calculable in perturbative QCD (pQCD).

Thus, the investigation of the internal structure of jets gives insight into the transition between the parton produced in the hard process and the experimentally observed jet of hadrons. QCD predicts that *(i)* the jet substructure is driven by gluon emission off primary partons at sufficiently high jet transverse energy, $E_T^{\rm jet}$, where fragmentation effects become negligible, *(ii)* jets originating from gluons are broader than those originating from quarks since the gluon-initiated jets radiate more due to their larger colour charge and *(iii)* the jet substructure depends mainly on the type of primary parton (quark or gluon) from which it originated and to a lesser extent on the hard scattering process. The experimental results from HERA which confirm these predictions are presented in this report.

The jet substructure can be studied in terms of two different observables, namely the jet shape [1] and the subjet multiplicity [2]. The jet shape is defined as the fraction of the jet transverse energy that lies inside a cone in the $\eta-\phi$ plane of radius r, $E_T(r)$, concentric with the jet axis. The mean integrated jet shape is given by

$$\langle\psi(r)\rangle = \frac{1}{N_{\rm jets}} \sum_{\rm jets} \frac{E_T(r)}{E_T^{\rm jet}}.$$

To compute the jet shape, the jets can be reconstructed either with the cone [3] or the k_T [4] algorithms. In contrast, the subjet multiplicity can be computed using only the jets reconstructed with the k_T algorithm and is obtained by reapplying the algorithm until for every pair of particles inside the jet, the quantity

---

*Talk given in the "Ringberg Workshop: New Trends in HERA Physics 2008", Ringberg Castle, Tegernsee, Germany, October 2008.

$$d_{ij} = \min(E_{Ti}, E_{Tj})^2[(\eta_i - \eta_j)^2 + (\phi_i - \phi_j)^2]$$

is above $y_{\rm cut} \cdot (E_T^{\rm jet})^2$, where $y_{\rm cut}$ is the resolution parameter. The mean subjet multiplicity is given by

$$\langle n_{\rm sbj}(y_{\rm cut})\rangle = \frac{1}{N_{\rm jets}} \sum_{i=1}^{N_{\rm jets}} n^i_{\rm sbj}(y_{\rm cut}).$$

The calculations of the jet substructure using QCD-based leading-order (LO) Monte Carlo (MC) models, such as Pythia [5], Herwig [6], Ariadne [7] and Lepto [8], are approximations based on a parton-shower approach. In fixed-order QCD calculations, the lowest order provides no structure for the jets since there is only one parton inside a jet. Higher-order terms give the lowest non-trivial contribution to the jet substructure. In particular, it is possible to obtain next-to-leading-order (NLO) calculations for jet substructure in neutral current (NC) deep inelastic scattering (DIS) in the laboratory frame from $\mathcal{O}(\alpha_s^2)$ predictions since, in this case, three partons can be inside one jet. Thus, measurements of jet substructure provide a stringent test of pQCD directly beyond LO. The pQCD calculations of the jet shape and subjet multiplicity are obtained via

$$\langle 1 - \psi(r)\rangle = \frac{\int_r^R dE_T\ (E_T/E_T^{\rm jet})[d\sigma(ep \to 2{\rm partons})/dE_T]}{\sigma_{\rm jet}(E_T^{\rm jet})}$$

$$\langle n_{\rm sbj}(y_{\rm cut})\rangle = 1 + \frac{1}{\sigma_{\rm jet}} \sum_{j=2}^{\infty} (j-1) \cdot \sigma_{{\rm sbj},j}(y_{\rm cut}) = 1 + C_1\ \alpha_s + C_2\ \alpha_s^2.$$

2. Tests of pQCD using jet substructure

At HERA, the main source of jets is photoproduction. At LO QCD, two processes contribute to the jet production cross section, resolved, in which the photon interacts via its partonic structure, and direct processes, in which the photon interacts as a point-like particle. Both processes give rise to two jets in the final state. The observable $x_\gamma^{\rm obs} \equiv (1/E_\gamma)(\sum_{\rm jets} E_T^{\rm jet} e^{-\eta^{\rm jet}})$ measures the energy invested by the photon in producing the dijet system and can be used to separate resolved and direct processes since they populate different regions of phase space. Resolved processes give rise to jets of quarks and gluons in the final state. On the other hand, direct processes are dominated by quark jets, so the $\eta^{\rm jet}$ dependence of the jet substructure is expected to show quark-like jets in the rear direction and gluon-like jets in the proton direction due to HERA dynamics, since for the dominant resolved diagram ($g_p q_\gamma \to gq$), the gluon goes forward. On the other hand, the jets in an inclusive-jet sample of NC or charged current (CC) DIS processes are dominated by quark jets so that no significant dependence with $\eta^{\rm jet}$ is expected. Only for a dijet sample, which contains a larger fraction of gluon jets, some dependence with $\eta^{\rm jet}$ could be observed.

The mean integrated jet shape was measured [9] for inclusive-jet photoproduction using the iterative cone algorithm with cone radius $R = 1$. Figure 1 shows the mean integrated jet shape as a function of r for different regions of $\eta^{\rm jet}$. The jets become broader as $\eta^{\rm jet}$ increases. The comparison with the QCD-based MC calculations shows that models with only fragmentation predict jets that are too narrow compared to the data. In contrast, models which include initial- and final-state QCD radiation describe the data well for $-1 < \eta^{\rm jet} < 1$. Therefore, parton radiation is the dominant mechanism responsible for the jet shape.

The comparison of the measurements with predictions for samples of pure quark- or gluon-initiated jets (see Fig. 2) shows that the measured jets are quark-like for $-1 < \eta^{\rm jet} < 0$ and become increasingly gluon-like as $\eta^{\rm jet}$ increases, as predicted by QCD.

To see more clearly the dependence of the jet shape with $\eta^{\rm jet}$ and $E_T^{\rm jet}$, the mean integrated jet shape as a function of $\eta^{\rm jet}$ and $E_T^{\rm jet}$ for a fixed value of $r = 0.5$ [10] is presented in Fig. 3. This analysis was done using the k_T algorithm to re-

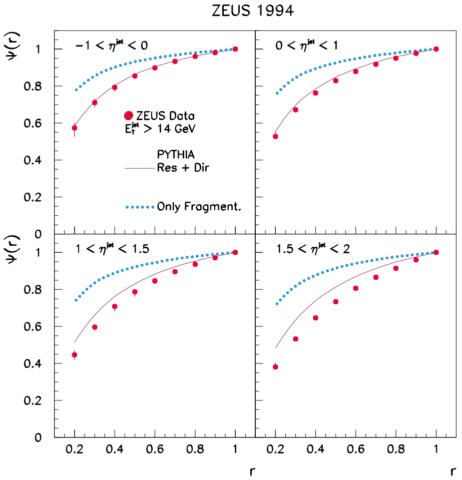

Figure 1. Mean integrated jet shape in inclusive-jet photoproduction.

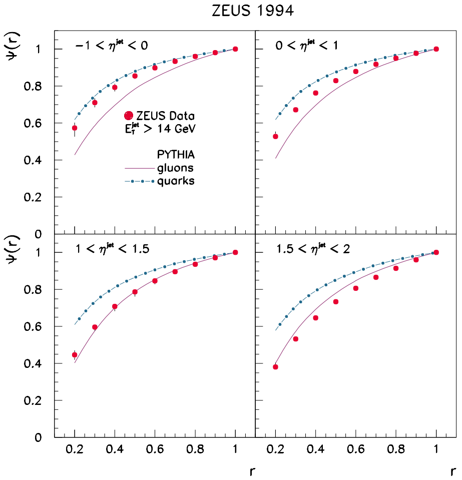

Figure 2. Mean integrated jet shape in inclusive-jet photoproduction.

construct the jets. The measured jet shape decreases as $\eta^{\rm jet}$ increases, which indicates that the jets become broader, and the measured jet shape increases as $E_T^{\rm jet}$ increases, which indicates that the jets become narrower as $E_T^{\rm jet}$ increases. The comparison with the predictions for quark and gluon jets shows that the broadening of the jets as $\eta^{\rm jet}$ increases is consistent with an increasing fraction of gluon jets. The comparison with the predictions for resolved and direct processes shows that the events are dominated by resolved processes at low $E_T^{\rm jet}$, whereas the direct contribution becomes increasingly more important as $E_T^{\rm jet}$ increases.

This last result was studied in more detail [11] by separating a dijet photoproduction sample in $x_\gamma^{\rm obs} < 0.75$, dominated by resolved processes, and $x_\gamma^{\rm obs} > 0.75$, dominated by direct processes. The jets in the resolved-enriched sample are broader than those for the direct-enriched sample (see Fig. 4). The QCD-based MC predictions give a good description of the data and show that the data is consistent with being dominated by resolved (direct) processes for $x_\gamma^{\rm obs} < 0.75$ ($x_\gamma^{\rm obs} > 0.75$).

The mean integrated jet shape was also measured in NC DIS in the Breit frame for different regions of jet pseudorapidity, $\eta_{\rm B}^{\rm jet}$, and transverse energy, $E_{T,{\rm B}}^{\rm jet}$, for a sample of dijet events [12]. The measurements show that the jet shape for a fixed value of $r = 0.5$ decreases as a function of $\eta_{\rm B}^{\rm jet}$. The effect is more pronounced at low $E_{T,{\rm B}}^{\rm jet}$ (see Fig. 5). The data are well described by the predictions of the QCD-based MC models; this comparison shows that the observed jet substructure is compatible with that of quark-initiated jets.

Figures 6 and 7 show the integrated jet shape measured in NC DIS in the laboratory frame for a sample of inclusive jets as a function of r in different regions of $\eta^{\rm jet}$ and $E_T^{\rm jet}$ [10]. The measurements are compared to NLO calculations [13], which give a good description of the data for $r > 0.1$. The $\eta^{\rm jet}$ and $E_T^{\rm jet}$ dependence of the mean integrated jet shape was measured for a fixed value of $r = 0.5$ (see Fig. 8). No significant variation with $\eta^{\rm jet}$ is observed in this case, consistent with the sample being dominated by quark jets in all the phase space measured. It is observed that the jets become narrower as $E_T^{\rm jet}$ increases. The NLO calculations give a good description of the data and show a sensitivity to the value of α_s. From the measured jet shape for $E_T^{\rm jet} > 21$ GeV, a value of $\alpha_s(M_Z)$ was extracted, $\alpha_s(M_Z) = 0.1176 \pm 0.0009\ ({\rm stat.})\ ^{+0.0009}_{-0.0026}\ ({\rm exp.})\ ^{+0.0091}_{-0.0072}\ ({\rm th.})$, which is consistent with other determinations from more inclusive channels and has a small experimen-

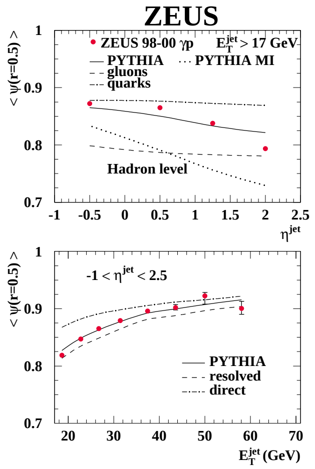

Figure 3. Mean integrated jet shape in inclusive-jet photoproduction.

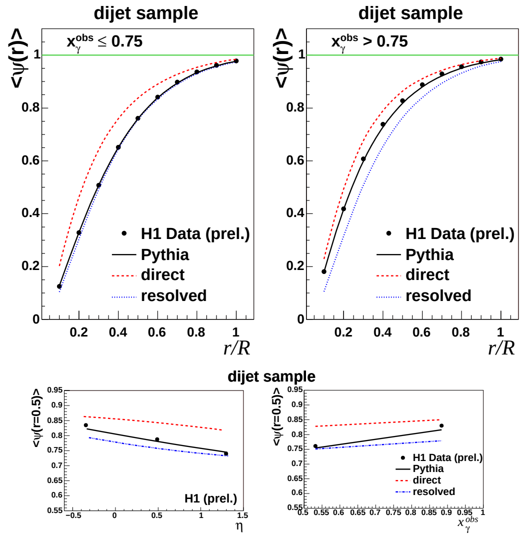

Figure 4. Mean integrated jet shape in dijet photoproduction.

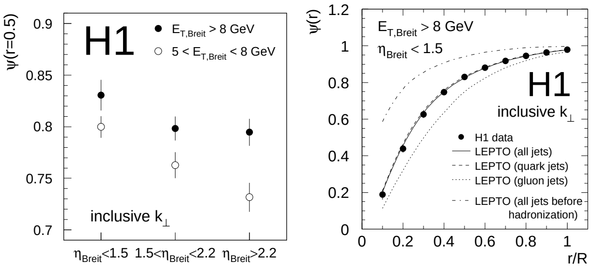

Figure 5. Mean integrated jet shape in dijet NC DIS in the Breit frame.

tal uncertainty. The theoretical uncertainties are dominant, especially that arising from higher orders; a better determination of α_s from this observable would be possible once higher-order corrections for NC DIS become available.

The mean subjet multiplicity has been measured in inclusive-jet photoproduction [10], dijets in NC DIS [12] and inclusive-jets in NC DIS [14] (see Fig. 9). The conclusions are similar to those from the integrated jet shape. In addition, a value of $\alpha_s(M_Z)$ was extracted from this observable in NC DIS: $\alpha_s(M_Z) = 0.1187 \pm 0.0017 \text{ (stat.) } ^{+0.0024}_{-0.0009} \text{ (exp.) } ^{+0.0093}_{-0.0076} \text{ (th.)}$ [14].

3. Jet properties in different hard scattering processes

The measurements of the integrated jet shape in photoproduction and NC DIS were compared in order to study the properties of jets in different hard scattering processes [15]. Figure 10a shows the comparison of the jet shape in inclusive-jet NC DIS and dijets in photoproduction with $x_\gamma^{\rm obs} \leqslant 0.75$ as a function of r. It is observed that the jets in NC DIS, which are dominated by quark jets, are narrower than those in resolved photoproduction, which include a larger fraction of gluon jets, and similar to those in direct photoproduction, which are also dominated by quark jets. Figure 10b shows the integrated jet shape for $r = 0.5$ as a function of $\eta^{\rm jet}$ for samples of inclusive jets in photoproduction, dijets with $x_\gamma^{\rm obs} > 0.75$ in photoproduction and inclusive jets in NC DIS. The inclusive-jet photoproduction sample shows a behaviour which is consistent with an increasing fraction of gluon jets as $\eta^{\rm jet}$ increases, whereas the dijets with $x_\gamma^{\rm obs} > 0.75$ and the NC DIS samples, which come predominantly from quark jets, show no significant dependence with $\eta^{\rm jet}$.

The parton composition of the final state was studied in more detail by comparing the $\eta^{\rm jet}$ and $E_T^{\rm jet}$ dependence of samples of inclusive jets in photoproduction and NC DIS with the predictions of pure quarks and gluons [10] (see Fig. 11). The NC DIS sample is consistent with being dom-

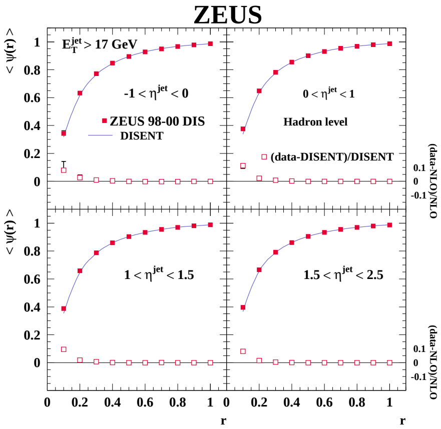

Figure 6. Mean integrated jet shape in inclusive-jet NC DIS in the laboratory frame.

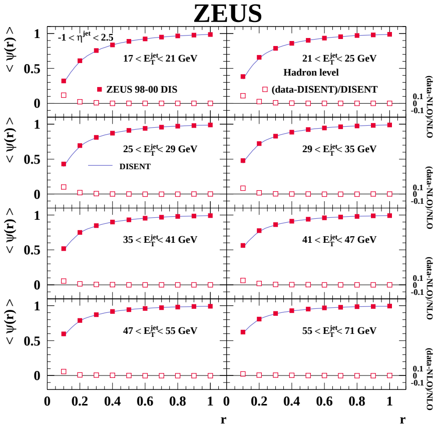

Figure 7. Mean integrated jet shape in inclusive-jet NC DIS in the laboratory frame.

inated by quark jets in the whole phase-space region. The jets in the photoproduction sample are similar to those of NC DIS for low $\eta^{\rm jet}$ and become increasingly broader as $\eta^{\rm jet}$ increases, which is consistent with the increase of the fraction of gluon jets. For the $E_T^{\rm jet}$ dependence, the NC DIS jets are well described by the prediction of quark jets in the whole measured range. The jets in the photoproduction sample get narrower somewhat faster than those in NC DIS.

The jets in the NC DIS sample were also compared to those of an inclusive-jet sample in CC DIS [16], also dominated by quark jets, so a similar dependence with e.g. $E_T^{\rm jet}$ is expected. Figure 12 shows the mean subjet multiplicity for a fixed value of $y_{\rm cut}$ as functions of $E_T^{\rm jet}$ and Q^2 in NC and CC DIS. The jets in both samples get narrower as $E_T^{\rm jet}$ increases, but the jets in CC seem to be slightly narrower than those in NC, in agreement with the NLO predictions [17]. These differences can be understood in terms of the different Q^2 spectra in NC and CC DIS.

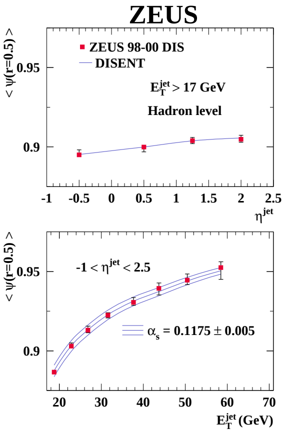

Figure 8. Mean integrated jet shape in inclusive-jet NC DIS in the laboratory frame.

The measurements in inclusive jets in NC DIS [15] were compared to similar measurements from CDF [18], DØ [19] and OPAL [20]. The jets in NC DIS and e^+e^- are similar (see Fig. 13), which is understood in terms of a similar parton composition of the final state, dominated by quark jets. The jets in NC DIS and e^+e^- are narrower than those in $p\bar{p}$ collisions, which can be understood from the fact that the final-state jets in $p\bar{p}$ come predominantly from gluons, as in resolved photoproduction. From these comparisons and the ones shown before, it can be concluded that the pattern of QCD radiation within a quark jet is to a large extent independent of the hard scattering process.

4. Quark- and gluon-jet properties

Several analyses were done at HERA in which quark and gluon jets were isolated and the dynamics of the underlying subprocesses studied. In some of these analyses, quark and gluon jets were

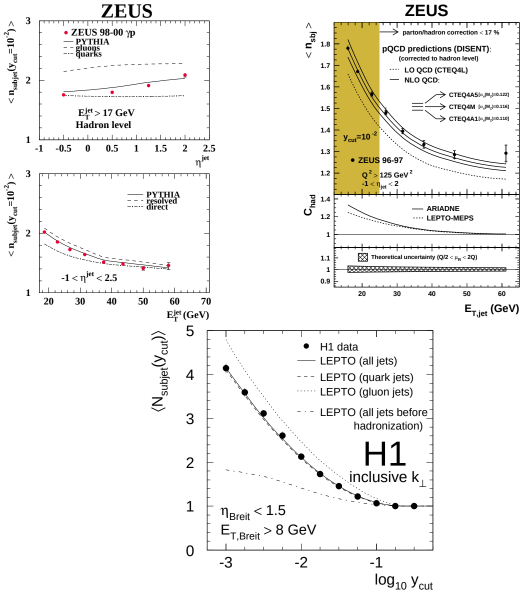

Figure 9. Mean subjet multiplicity in inclusive-jet photoproduction, inclusive-jet in NC DIS (laboratory frame) and dijet in NC DIS (Breit frame).

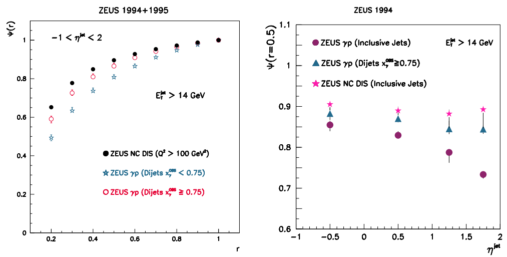

(a) (b)

Figure 10. Mean integrated jet shape in inclusive-jet and dijet in photoproduction and inclusive-jet in NC DIS.

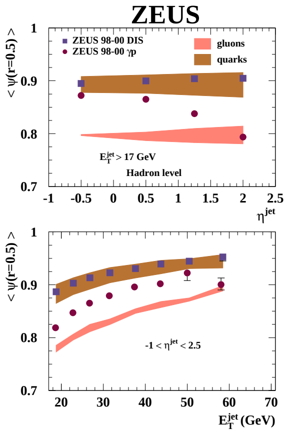

Figure 11. Mean integrated jet shape in inclusive-jet in photoproduction and NC DIS.

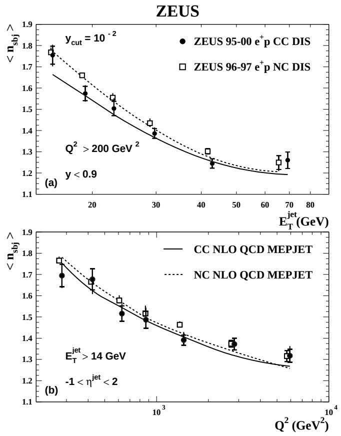

Figure 12. Mean subjet multiplicity in inclusive-jet in NC and CC DIS.

identified by using samples of dijet events in photoproduction which contain charm quarks in the final state. In these analyses, one of the jets is tagged as a charm and the substructure of the other ("untagged") jet was studied. This method provides an unbiased sample of quark jets. In direct photoproduction, the untagged jet is also a charm quark, but in resolved processes, since there are several contributing processes, such as gluon-gluon fusion or charm-excitation processes, the untagged jet can be a quark or a gluon.

The ZEUS Collaboration identified quark and gluon jets by selecting a sample of dijet events in photoproduction and tagging the subsample with charm production via the identification of a D^* meson associated with one of the jets [21]. The substructure of the untagged jet was measured and found to be consistent with the predictions for quark-initiated jets (see Fig. 14a). The substructure of gluon jets was extracted by means of $\mathcal{O}_{\rm dijet} = f_q \cdot \mathcal{O}_{\rm quark} + f_g \cdot \mathcal{O}_{\rm gluon}$, where the substructure of dijets is the measured observable, the substructure of quarks was approximated using the measured substructure of untagged charm jets and the fraction of quarks and gluons was estimated using the MC predictions, which de-

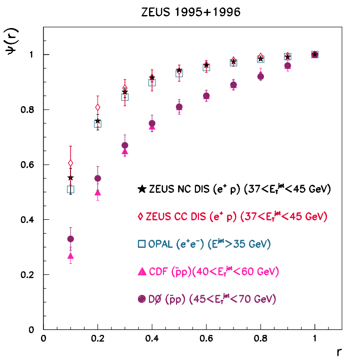

Figure 13. Mean integrated jet shape in inclusive-jet in e^+e^-, $p\bar{p}$ and NC and CC DIS.

scribe the data well. Figure 14b shows the extracted substructure of gluon jets compared with the measured substructure of untagged jets. The gluon jets are observed to be broader than the quark jets. The model predictions describe the measurements well.

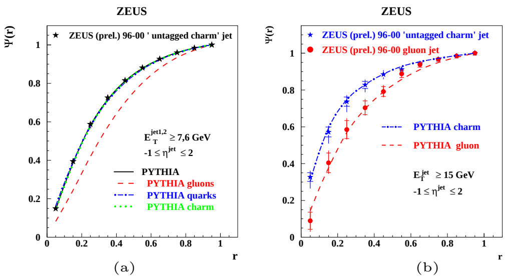

(a) (b)

Figure 14. Mean integrated jet shape in charm photoproduction.

The H1 Collaboration made a similar analysis, but tagging the charm jets by associating a muon to one of the jets [11]. The substructure of the other jet was studied for $x_\gamma^{\rm obs} \lesssim 0.75$ (see Fig. 15). The QCD-based MC predictions describe the data well for $x_\gamma^{\rm obs} > 0.75$. However, some differences are observed for $x_\gamma^{\rm obs} < 0.75$. The data suggest a smaller fraction of gluon jets, which can come only from the gluons in the charm-excitation subprocess, at low $x_\gamma^{\rm obs}$ than the predictions.

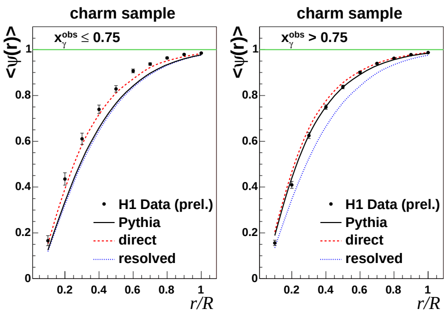

Figure 15. Mean integrated jet shape in charm photoproduction.

The differences between quark and gluon jets were also studied by exploiting the different type of parton content in the final state for one-jet and two-jet samples in NC DIS in the laboratory frame [22]. The one-jet sample is expected to be dominated by quark jets, whereas the two-jet sample is expected to contain a larger fraction of gluon jets. Figure 16 shows the measurement of the mean integrated jet shape as a function of r for $E_T^{\rm jet} > 14$ GeV and for $14 < E_T^{\rm jet} < 17$ GeV for the one-jet and the two-jet samples. For the two-jet sample, the substructure of the lowest-$E_T^{\rm jet}$ jet was studied for those events in which the two jets are closer than two units in the $\eta-\phi$ plane. These jets are observed to be broader than the jets in the one-jet sample. The data are compared to NLO calculations [13,23]. The calculations give a good description of the data and show that the measurements are consistent with a higher gluon content in the two-jet sample.

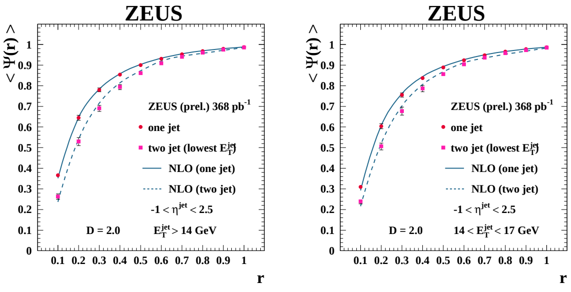

Figure 16. Mean integrated jet shape in one-jet and two-jet in NC DIS.

Since the QCD prediction that gluon jets are broader than quark jets has been amply proven by data, it is possible to exploit this fact for identifying the different type of jets and study the dynamics of the subprocesses. Quark and gluon jets were identified [10] on a statistical basis by selecting “narrow” and “broad” jets by requiring that the measured jet shape is smaller than 0.6 or larger than 0.8, respectively. Using this selection, the inclusive-jet cross section in photoproduction was measured as a function of $\eta^{\rm jet}$ (see Fig. 17). The measured cross section for broad jets displays a very different shape than that of the narrow jet sample. The $\eta^{\rm jet}$ distribution for the narrow jet sample peaks at about 0.5, whereas the broad jet sample distribution increases as $\eta^{\rm jet}$ increases. The predictions from the QCD-based MC models, with the same jet shape selection, give a good description of the shape of the data. The MC predicts that the broad jet sample is dominated by $qg \to qg$ via gluon exchange in resolved processes, whereas the narrow jet sample is dominated by boson-gluon fusion events in direct processes. Therefore, the narrow jet sample is indeed dominated by quark-initiated jets in the final state and the broad jet sample has a higher content of gluon-initiated jets. The comparison with the predictions for samples of pure quark or gluon jets supports this conclusion.

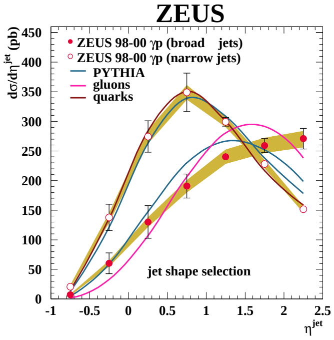

Figure 17. Inclusive-jet cross sections in photoproduction.

The underlying parton dynamics is reflected in the distribution of the scattering angle in the dijet centre-of-mass system, θ^*. The $\cos(\theta^*)$ distribution is sensitive to the spin of the exchanged particle: a different behaviour is expected for quark and gluon exchange. Samples selected according to the internal structure of the jets give an unbiased handle to explore the dynamics of the subprocesses. Figure 18a shows the dijet cross section as a function of $\cos(\theta^*)$ for samples of two broad or two narrow jets. The cross section for two broad jets rises more steeply than the sample of two narrow jets. The MC predictions give a reasonable description of the data. The different slope observed in the data can be understood in terms of the dominant subprocesses in the two samples: the two broad jet sample is dominated by subprocesses mediated by gluon exchange whereas the two narrow jet sample is dominated by subprocesses mediated by quark exchange. The $\cos(\theta^*)$ distribution for a sample of one narrow and one broad jet in the same event shows a clear asymmetry (see Fig. 18b). The MC reproduces the data well. The asymmetry observed can be understood in terms of the dominant subprocess: $qg \to qg$, the positive side is dominated by t-channel gluon exchange, whereas the negative side is dominated by u-channel quark exchange.

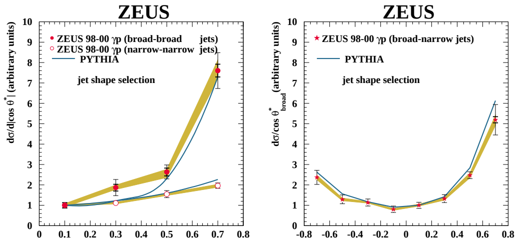

(a) (b)

Figure 18. Dijet cross sections in photoproduction.

5. The pattern of parton radiation

The pattern of parton radiation within a jet was studied using subjet distributions. The pattern of parton radiation from a primary parton is dictated in QCD by the splitting functions, so the measurements provide a direct test of these functions and their scale dependence. The subjet distributions can also be used to study colour-coherence effects between the initial and final states. QCD predicts that soft gluon radiation tends to be emitted towards the proton direction. The measurements of subjet distributions were done in NC DIS [24] as functions of the fraction of subjet transverse energy, $E_T^{\rm sbj}/E_T^{\rm jet}$, the difference between the η and ϕ of the subjet with respect to the jet, $\eta^{\rm sbj}-\eta^{\rm jet}$ and $|\phi^{\rm sbj}-\phi^{\rm jet}|$, and $\alpha^{\rm sbj}$, the angle, as viewed from the jet centre, between the subjet with higher-E_T and the proton beam line in the $\eta-\phi$ plane. The cross sections were measured for those jets which contain exactly two subjets for $y_{\rm cut} = 0.05$. Figure 19 shows the normalised subjet cross sections. The measurements show that the two subjets tend to have similar transverse energy. The distribution in $\eta^{\rm sbj}-\eta^{\rm jet}$ has a two-peak structure. The cross section as a function of $|\phi^{\rm sbj}-\phi^{\rm jet}|$ shows a suppression around $\Delta\phi = 0$, which comes from the fact that the two subjets cannot be resolved when they are too close together; this is also observed in the dip between the two peaks in $\eta^{\rm sbj}-\eta^{\rm jet}$. The $\alpha^{\rm sbj}$ distribution shows that the highest-E_T subjet tends to be in the rear direction. This is consistent with the asymmetric two peak structure observed in the $\eta^{\rm sbj}-\eta^{\rm jet}$ distribution and related to colour-coherence effects. NLO QCD predictions [13] are compared to the data and give an adequate description.

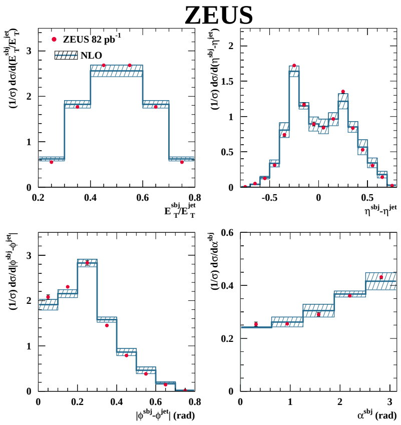

Figure 19. Normalised subjet cross sections in inclusive-jet NC DIS.

To study in more detail the colour-coherence effects, the cross section as a function $\eta^{\rm sbj}-\eta^{\rm jet}$ was measured for those jets with subjets of different transverse energy fraction, separately for the low- and high-E_T subjets. The measurements show that the high-E_T subjet tends to be in the rear whereas the low-E_T subjet tends to be emitted in the forward direction (see Fig. 20). The NLO predictions describe the data well. This behaviour can be attributed to colour-coherence effects between the initial and final states, and indicates that soft gluon radiation is emitted predominantly towards the proton direction.

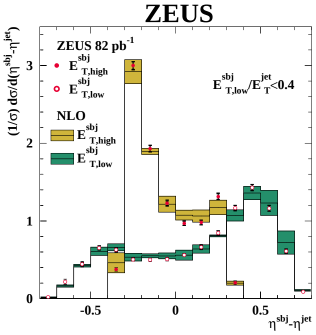

Figure 20. Normalised subjet cross sections in inclusive-jet NC DIS.

The pattern of parton radiation was further studied by comparing the predictions for quark- and gluon-induced splittings separately with the data. The NLO calculations predict that the rate is dominated by quark-induced processes. The predictions of these two types of processes have a different shape: the quark-induced processes have subjets with more similar transverse energy than the subjets from the gluon-induced processes, and the two subjets coming from a qg pair are closer together than in the case of $q\bar{q}$ pairs. The comparison with the measurements shows that the data are better described by the calculations for jets arising from the splitting of a quark into a qg pair (see Fig. 21).

6. Summary

Jet substructure has been extensively studied at HERA in terms of jet shapes and subjet multiplicities and distributions. The measurements performed allowed stringent tests of perturbative

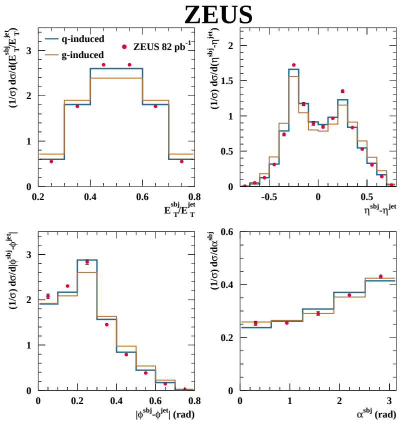

Figure 21. Normalised subjet cross sections in inclusive-jet NC DIS.

QCD directly beyond leading order, comparison of the properties of quark and gluon jets, the comparison of the pattern of QCD radiation in different hard scattering processes, determinations of the strong coupling, the study of the dynamics of the underlying subprocesses and the study of the pattern of parton radiation. Therefore, jet substructure provides a powerful tool to make stringent tests of perturbative QCD.

Acknowledgments. I would like to thank the organisers for giving me the opportunity of presenting these results and for a well organised conference.

REFERENCES

1. S.D. Ellis, Z. Kunszt and D.E. Soper, *Phys. Rev. Lett.* 69 (1992) 3615.
2. S. Catani et al., *Nucl. Phys.* **B** 383 (1992) 419.
3. CDF Collab., F. Abe et al., *Phys. Rev.* **D** 45 (1992) 1448.
4. S. Catani et al., *Nucl. Phys.* **B** 406 (1993) 187.
5. H.-U. Bengtsson and T. Sjöstrand, *Comp. Phys. Comm.* 46 (1987) 43; T. Sjöstrand, *Comp. Phys. Comm.* 82 (1994) 74.
6. G. Marchesini et al., *Comp. Phys. Comm.* 67 (1992) 465.
7. L. Lonnblad, *Comp. Phys. Comm.* 71 (1992) 15.
8. G. Ingelman, A. Edin and J. Rathsman *Comp. Phys. Comm.* 101 (1997) 108.
9. ZEUS Collab., J. Breitweg et al., *Eur. Phys. Jour.* **C** 2 (1998) 61.
10. ZEUS Collab., S. Chekanov et al., *Nucl. Phys.* **B** 700 (2004) 3.
11. H1 Collab., H1-prelim-05-077, 2005.
12. H1 Collab., C. Adloff et al., *Nucl. Phys.* **B** 545 (1999) 3.
13. S. Catani and M.H. Seymour, *Nucl. Phys.* **B** 485 (1997) 291.
14. ZEUS Collab., S. Chekanov et al., *Phys. Lett.* **B** 558 (2003) 41.
15. ZEUS Collab., J. Breitweg et al., *Eur. Phys. Jour.* **C** 8 (1999) 367.
16. ZEUS Collab., S. Chekanov et al., *Eur. Phys. Jour.* **C** 31 (2003) 149.
17. E. Mirkes and D. Zeppenfeld, *Phys. Lett.* **B** 380 (1996) 205.
18. CDF Collab., F. Abe et al., *Phys. Rev. Lett.* 70 (1993) 713.
19. DØ Collab., S. Abachi et al., *Phys. Lett.* **B** 357 (1995) 500.
20. OPAL Collab., R. Akers et al., *Z. Phys.* **C** 63 (1994) 197.
21. ZEUS Collab., contributed paper to "International Europhysics Conference on High Energy Physics", Budapest, Hungary, July 2001.
22. ZEUS Collab., ZEUS-prel-07-013, 2007.
23. Z. Nagy and Z. Trocsanyi, *Phys. Rev. Lett.* 87 (2001) 082001.
24. ZEUS Collab., S. Chekanov et al., DESY 08-178, December 2008.